AN UPPER BOUND SOLUTION OF BACKWARD TUBE EXTRUSION PROCESS THROUGH CURVED PUNCHES

Heshmatollah Haghighat[1)], Gholam Reza Asgari[2)]*
[1)] Mechanical Engineering Department, Razi University, Kermanshah, Iran
[2)] Golpayegan Payam Non-Governmental Institute of Higher Education, Golpayegan, Iran

Received: 30.10.2012
Accepted: 11.11.2013

[*]Corresponding author: e-mail: hhaghighat@razi.ac.ir, Tel.: +98-831- 4274530, Mechanical Engineering Department, Razi University, Kermanshah, Iran

Abstract
In this paper, an upper bound approach is used to analyze the process of backward tube extrusion through arbitrarily curved punches. Based on the assumptions of proportional angles and proportional distances from the mandrel surface in the deformation zone, two kinematically admissible velocity fields are proposed and those are used in upper bound solution. By using the developed upper bound solution, optimum punch lengths which minimize the extrusion forces are determined for a streamlined punch shape and also for a conical punch. The corresponding results are also determined by using a finite element code, ABAQUS, and by doing some experiments and compared with the analytical results. This comparisons show a good agreement.

Keywords: Backward tube extrusion, Upper bound, Experiment

1 Introduction

In backward extrusion, there is no relative movement between the initial billet and the container and it is characterized by the absence of friction between the initial billet surface and the container. This process needs lower extrusion force and also it is suitable for producing partially extruded products because of the simplicity in ejecting of the extruded part from the container as compared with forward extrusion process. In this process, such as other metal forming processes, calculation and optimization of extrusion force are important. Among various analytical and numerical approximate methods of solution, the upper bound technique and the finite element method have been widely used for the analysis of the extrusion process. One of the limitations of most of the current FEM solution schemes for metal forming is that they do not provide parametric analysis. Hence, any parametric investigation is usually done manually by changing one FE model to another until a feasible solution is obtained. Establishment of analytical solutions for extrusion process facilitates parametric study and may help in understanding the mechanics behind the extrusion processes better. Even though the finite element gives detailed information, it takes considerable CPU time. Using the upper-bound technique has the merits of saving computer's CPU and it appears to be a useful tool for analyzing metal forming problems when the objective of such an analysis is limited to prediction of deformation load and/or to study metal flow during the process. A number of people have used the upper bound method to analyze the extrusion process. Avitzur [1-3] developed models for forward rod extrusion through conical dies using the upper bound approach. Chen and Ling [4] developed a velocity field for axisymmetric extrusions through cosine, elliptic and

DOI 10.12776/ams.v20i1.214 p-ISSN 1335-1532
e-ISSN 1338-1156

hyperbolic dies. Zimmerman and Avitzur [5] also modeled extrusion using the upper bound method with generalized shear boundaries. Mehta et al. developed a kinematically admissible velocity field and compared it with the experimentally obtained flow field using the visio-plasticity technique [6]. Chang and Choi developed an upper bound solution for tube extrusion through curved dies [7]. Hartley proposed a kinematically admissible velocity field for forward tube extrusion through a conical die, which reduces to the kinematically admissible velocity field for rod extrusion in the limit as the mandrel diameter goes to zero [8]. Yang et al. [9] as well as Yang and Han [10] developed upper bound models for forward rod extrusion with streamlined dies. An upper bound solution for strain hardening materials has been developed by Yang et al. for tube extrusion through streamlined dies [11]. They extended the same analysis for three-dimensional forward extrusion of arbitrarily shaped tubes [12]. Altan proposed a deformation model for tube extrusion through a flat die by assuming the flow lines to be straight [13]. Bakhshi et al. proposed an optimum punch profile in backward rod extrusion [14]. Saboori et al. studied the energy consumption in forward and backward rod extrusion [15]. A feature based upper bound model to analyze the backward tube extrusion proposed by Malpani and Kumar [16]. The analysis was based on a kinematically admissible velocity field to obtain the optimal extrusion pressure by optimizing the die length. Ebrahimi et al. [17] proposed a kinematically admissible velocity field for forward tube extrusion through conical dies. Gordon et al. were developed an adaptable die design method for forward rod extrusion and described them in details in a series of papers [18-20].

The purpose of this paper is to develop a velocity field that applicable to backward tube extrusion through arbitrarily curved punches. The proposed velocity field is used to find out an optimal streamlined punch length and the corresponding extrusion force for a given process conditions. The investigation is also performed using the finite element code, ABAQUS and by doing some experiments.

2 Upper bound analysis

Fig. 1 shows a schematic diagram of the tube backward extrusion through an arbitrarily shaped punch with fixed cylindrical shaped mandrel. In this figure R_o and R_f are outer radii of the initial and the extruded tube and R_m is the mandrel radius. To analyze the process by using the upper bound method, the material under deformation is divided into three zones. In zone I, material is stationary and in zone III the material moves rigidly with the velocity V_f. Zone II is surrounded by two velocity discontinuity surfaces S_1, S_2, mandrel surface and the punch surface. The punch surface, which is labeled as $\psi(r)$ in Fig. 1, is given in the spherical coordinate system, (r,θ,ϕ), where $\psi(r)$ is the angular position of the punch surface as a function of the radial distance from the origin. The origin of spherical coordinate system is located at point O which is defined by the intersection of the axis of symmetry with the line that goes through the point where the punch begins and the exit point of the punch. The

spherical velocity discontinuity surface S_1 is located at distance r_o from the origin and the spherical velocity discontinuity surface S_2 is located at distance r_f from the origin.

From Fig. 1, we have

$$R_o = R_m + r_o \sin\alpha\,,\ R_f = R_m + r_f \sin\alpha \tag{1}$$

where α is the angle of the line connecting the initial point of the curved punch to the final point of the punch and $\tan\alpha = (R_o - R_f)/L$, where L is punch length.

The exit velocity V_f is determined by

DOI 10.12776/ams.v20i1.214 p-ISSN 1335-1532
e-ISSN 1338-1156

$$V_f = \frac{{R_o}^2 - {R_f}^2}{{R_f}^2 - {R_m}^2} V_o \tag{2}$$

Substituting Eq. (2) into Eq. (3), the exit velocity V_f can be written as

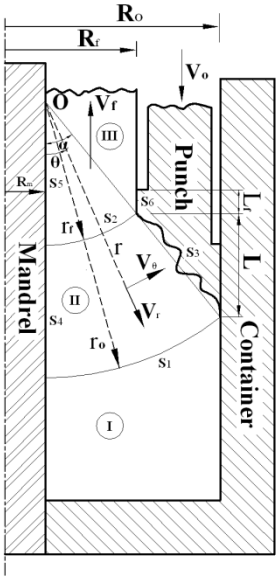

Fig. 1 Schematic diagram showing backward tube extrusion through an arbitrarily curved punch.

$$V_f = \frac{(R_m + r_o \sin\alpha)^2 - (R_m + r_f \sin\alpha)^2}{(R_m + r_f \sin\alpha)^2 - {R_m}^2} V_o \tag{3}$$

For small radius of the mandrel, the above equation can be simplified as

$$V_f \cong (\frac{{r_o}^2}{{r_f}^2} - 1) V_o \tag{4}$$

The first step in the upper bound analysis is to choose an admissible velocity field for the material undergoing plastic deformation. The assumption of velocity field will influence the prediction of load and metal flow. The velocity field that has been derived from incompressibility condition and satisfies the velocity boundary conditions is a kinematically admissible velocity field.

2.1 Velocity field in the deformation zone

Two assumptions that were used by Gordon et al. [18] for forward rod extrusion are used here for backward tube extrusion process. If the assumption of proportional angles in the deformation zone is made, then radial velocity component is written as

DOI 10.12776/ams.v20i1.214 p-ISSN 1335-1532
e-ISSN 1338-1156

$$V_r = V_o \cos\theta - \frac{V_o}{2}\left(\frac{r_o}{r}\right)^2 \frac{\alpha}{\psi}\frac{\sin(2\theta\alpha/\psi)}{\sin\theta} \tag{5}$$

Assuming the proportional distance from the mandrel surface then

$$V_r = V_o \cos\theta - V_o\left(\frac{r_o}{r}\right)^2 \frac{\sin^2\alpha}{\sin^2\psi}\cos\theta \tag{6}$$

The full velocity field for the flow of the material in deformation zone is obtained by invoking volume constancy. Volume constancy in spherical coordinate system is defined as

$$\dot{\varepsilon}_{rr} + \dot{\varepsilon}_{\theta\theta} + \dot{\varepsilon}_{\phi\phi} = 0 \tag{7}$$

where $\dot{\varepsilon}_{ii}$ is the normal strain rate component in the i-direction. The strain rates in spherical coordinates are defined as

$$\dot{\varepsilon}_{rr} = \frac{\partial V_r}{\partial r}$$

$$\dot{\varepsilon}_{\theta\theta} = \frac{1}{r}\frac{\partial V_\theta}{\partial \theta} + \frac{V_r}{r}$$

$$\dot{\varepsilon}_{\phi\phi} = \frac{1}{r\sin\theta}\frac{\partial V_\phi}{\partial \phi} + \frac{V_r}{r} + \frac{V_\theta}{r}\cot\theta$$

$$\dot{\varepsilon}_{r\theta} = \frac{1}{2}\left(\frac{\partial V_\theta}{\partial r} - \frac{V_\theta}{r} + \frac{1}{r}\frac{\partial V_r}{\partial \theta}\right)$$

$$\dot{\varepsilon}_{\theta\phi} = \frac{1}{2}\left(\frac{1}{r\sin\theta}\frac{\partial V_\theta}{\partial \phi} + \frac{1}{r}\frac{\partial V_\phi}{\partial \theta} - \frac{\cot\theta}{r}V_\phi\right)$$

$$\dot{\varepsilon}_{\phi r} = \frac{1}{2}\left(\frac{\partial V_\phi}{\partial r} - \frac{V_\phi}{r} + \frac{1}{r\sin\theta}\frac{\partial V_r}{\partial \phi}\right) \tag{8}$$

For the axisymmetric extrusion (i.e. $V_\phi = 0$) and the angular component of velocity, V_θ is obtained by placing V_r, from Eqs. (5)-(6) into Eqs. (7)-(8), solving for V_θ and applying appropriate boundary conditions. Then, there are two velocity fields depending on the mentioned assumptions:

(1) Assuming proportional angles in the deformation zone:

$$V_r = V_o \cos\theta - \frac{V_o}{2}\left(\frac{r_o}{r}\right)^2 \frac{\alpha}{\psi}\frac{\sin(2\theta\alpha/\psi)}{\sin\theta}$$

$$V_\theta = -V_o \sin\theta - \frac{V_o}{2}\frac{{r_o}^2}{r}\frac{\partial\psi}{\partial r}\frac{\alpha\theta}{\psi^2}\frac{\sin(2\theta\alpha/\psi)}{\sin\theta}$$

DOI 10.12776/ams.v20i1.214 p-ISSN 1335-1532
e-ISSN 1338-1156

$$V_\varphi = 0 \tag{9}$$

(2) Assuming the proportional distances from the mandrel surface:

$$V_r = V_o \cos\theta - V_o\left(\frac{r_o}{r}\right)^2 \frac{\sin^2\alpha}{\sin^2\psi}\cos\theta$$

$$V_\theta = -V_o \sin\theta - V_o \frac{r_o^{\,2}}{r}\left(\frac{\sin\alpha}{\sin\psi}\right)^2 \frac{\partial\psi}{\partial r}\frac{\sin\theta}{\tan\psi}$$

$$V_\varphi = 0 \tag{10}$$

If the exit velocity V_f is determined by Eq. (4), then Eqs. (9)-(10) satisfy the incompressibility condition and the boundary conditions on velocity discontinuity surfaces S_1, S_2 and mandrel surface as well as the punch surface. Therefore, they are deemed to be kinematically admissible fields.

Based on the proposed velocity fields, the strain rate fields for deformation zone can be obtained by Eq. (9). With the strain rate field and the velocity field, the standard upper bound method can be implemented. This upper bound model involves calculating the internal power of deformation over the deformation zone volume, calculating the shear power losses over the surfaces of velocity discontinuity, and the frictional power losses along frictional surfaces. Since, no deformation occurs in zones I and III, therefore, the strain rate components are zero.

2.2 Internal power of deformation

The internal power of deformation in an upper bound model is

$$\dot{W}_i = \frac{2\sigma_0}{\sqrt{3}}\int_v \sqrt{\frac{1}{2}\dot{\varepsilon}_{ij}\dot{\varepsilon}_{ij}}\,dV \tag{11}$$

Internal power of zones I and III are zero and the equation to calculate the internal power of deformation in zone II is

$$\dot{W}_i = \frac{4\pi\sigma_0}{\sqrt{3}}\int_{r_f}^{r_o}\int_0^{\psi(r)} \sqrt{\frac{1}{2}(\dot{\varepsilon}_{rr}^2 + \dot{\varepsilon}_{\theta\theta}^2 + \dot{\varepsilon}_{\varphi\varphi}^2) + \dot{\varepsilon}_{r\theta}^2}\;(R_m + r\sin\theta)\,r\,d\theta\,dr \tag{12}$$

where σ_0 is the mean flow stress of material and is given by

$$\sigma_0 = \frac{\int_0^{\varepsilon}\sigma\,d\varepsilon}{\varepsilon}, \qquad \varepsilon = \ln\frac{R_o^2 - R_f^2}{R_f^2 - R_m^2} \tag{13}$$

2.3 Shear power losses

The equation for the power losses along a shear surface of velocity discontinuity is

$$\dot{W}_S = \frac{\sigma_0}{\sqrt{3}}\int_{S_v}|\Delta V|\,dS \tag{14}$$

DOI 10.12776/ams.v20i1.214 p-ISSN 1335-1532
e-ISSN 1338-1156

The shear power losses along the velocity discontinuity surfaces S_1 and S_2 with assuming proportional angles in the deformation zone, become

$$\dot{W}_{S1} = \frac{2\pi\sigma_0}{\sqrt{3}} V_o\, r_o \int_0^{\alpha} (\sin\theta + r_o \frac{\theta}{\alpha} \cos\theta \frac{\partial\psi}{\partial r}\Big|_{r=r_o})(R_m + r_o \sin\theta)\, d\theta \tag{15}$$

$$\dot{W}_{S2} = \frac{2\pi\sigma_0}{\sqrt{3}} V_o \frac{{r_o}^2}{r_f} \int_0^{\alpha} (\sin\theta + r_f \frac{\theta}{\alpha} \cos\theta \frac{\partial\psi}{\partial r}\Big|_{r=r_f})(R_m + r_f \sin\theta)\, d\theta \tag{16}$$

and with assuming the proportional distances from the mandrel surface, become

$$\dot{W}_{S1} = \frac{2\pi\sigma_0}{\sqrt{3}} V_o\, r_o \int_0^{\alpha} (1 + r_o (\frac{\sin\alpha}{\sin\psi})^2 \frac{1}{\tan\psi} \frac{\partial\psi}{\partial r}\Big|_{r=r_o})(R_m + r_o \sin\theta)\, d\theta \tag{17}$$

$$\dot{W}_{S2} = \frac{2\pi\sigma_0}{\sqrt{3}} V_o \frac{{r_o}^2}{r_f} \int_0^{\alpha} (1 + r_f (\frac{\sin\alpha}{\sin\psi})^2 \frac{1}{\tan\psi} \frac{\partial\psi}{\partial r}\Big|_{r=r_f})(R_m + r_f \sin\theta)\sin\theta\, d\theta \tag{18}$$

2.4 Friction power losses

The general equation for the friction power losses for a surface with a constant friction factor m is

$$\dot{W}_f = m \frac{\sigma_0}{\sqrt{3}} \int_{S_f} |\Delta V|\, dS \tag{19}$$

For punch surface S_3 the differential surface and the magnitude of the velocity difference are

$$dS = 2\pi(R_m + r\sin\psi)\sqrt{1 + (r\frac{\partial\psi}{\partial r})^2}\, dr \tag{20}$$

$$|\Delta V| = |(V_r - V_o\cos\psi)\cos\eta + (V_\theta + V_o\sin\psi)\sin\eta|_{\theta=\psi} \tag{21}$$

where η is local angle of the punch surface with respect to the local radial velocity component and

$$\cos\eta = \frac{1}{\sqrt{1 + (r\frac{\partial\psi}{\partial r})^2}}, \quad \sin\eta = \frac{r\frac{\partial\psi}{\partial r}}{\sqrt{1 + (r\frac{\partial\psi}{\partial r})^2}} \tag{22}$$

$$\dot{W}_{f3} = \frac{\pi\sigma_0}{\sqrt{3}} m V_o {r_o}^2 \sin 2\alpha \int_{r_f}^{r_o} \left| \frac{\alpha}{\psi\sin\psi} (\frac{1}{r^2} + (\frac{\partial\psi}{\partial r})^2) \right| (R_m + r\sin\psi)\, dr \tag{23}$$

DOI 10.12776/ams.v20i1.214 p-ISSN 1335-1532
e-ISSN 1338-1156

The frictional power losses along the surface S_4, shown in Fig. 1, with assuming proportional angles in the deformation zone is calculated as

$$\dot{W}_{f4} = \frac{2\pi\sigma_0}{\sqrt{3}} m V_o R_m \int_{r_f}^{r_o} \left| 1 - (\frac{r_o}{r})^2 (\frac{\alpha}{\psi})^2 \right| dr \tag{24}$$

and with assuming the proportional distances from the mandrel surface, it becomes

$$\dot{W}_{f4} = \frac{2\pi\sigma_0}{\sqrt{3}} m V_o R_m \int_{r_f}^{r_o} \left| 1 - (\frac{r_o}{r})^2 (\frac{\sin\alpha}{\sin\psi})^2 \right| dr \tag{25}$$

The frictional power losses along the surface S_5 can be given by

$$\dot{W}_{f5} = \frac{2\pi}{\sqrt{3}} m\sigma_0 R_m V_f r_f \tag{26}$$

Finally, the power dissipated on the frictional surface S_6, punch land, becomes

$$\dot{W}_{f6} = \frac{2\pi}{\sqrt{3}} m\sigma_0 R_f (V_f - V_o) L_f \tag{27}$$

where L_f is the length of the punch land.
Based on the upper bound model, the total power needs for backward tube extrusion process is obtained by summing the internal power and the power dissipated on all frictional and velocity discontinuity surfaces. Therefore, the total upper bound solution for the relative extrusion pressure is given by

$$\frac{P_{aver}}{\sigma_0} = \frac{\dot{W}_i + \dot{W}_{S1} + \dot{W}_{S2} + \dot{W}_{f3} + \dot{W}_{f4} + \dot{W}_{f5} + \dot{W}_{f6}}{\pi(R_o^2 - R_f^2) V_o \sigma_0} \tag{28}$$

A MATLAB program has been implemented for the previously derived equations and is used to study the backward tube extrusion process for different punch shapes and different process conditions. It includes a parameter L, punch length, which should be optimized.

3 Comparison of the velocity fields

The developed velocity fields and the upper bound model can be used for backward tube extrusion through punches of any shape if the punch profile is expressed as equation $\psi(r)$. To compare the upper bound results obtained for the two velocity fields, the die profile introduced by Yang and Han [9, 10] for forward rod extrusion is selected for the profile of the punch. They created a streamlined die shape as a fourth-order polynomial whose slope is parallel to the axis at both entrance and exit of the die. Die shape of Yang and Han can be expressed in spherical coordinate system, shown in Fig. 1, as

DOI 10.12776/ams.v20i1.214 p-ISSN 1335-1532
e-ISSN 1338-1156

$$\frac{r}{r_o}\frac{\sin\psi}{\sin\alpha}=1+\left(\frac{C_f}{(1-\frac{R_f-R_m}{R_o-R_m})^2}-\frac{3}{1-\frac{R_f-R_m}{R_o-R_m}}\right)\left(-\frac{r}{r_o}\frac{\cos\psi}{\cos\alpha}+1\right)^2$$
$$+\left(\frac{2}{(1-\frac{R_f-R_m}{R_o-R_m})^2}-\frac{2C_f}{(1-\frac{R_f-R_m}{R_o-R_m})^3}\right)\left(-\frac{r}{r_o}\frac{\cos\psi}{\cos\alpha}+1\right)^3 \quad (29)$$
$$+\frac{C_f}{(1-\frac{R_f-R_m}{R_o-R_m})^4}\left(-\frac{r}{r_o}\frac{\cos\psi}{\cos\alpha}+1\right)^4$$

where

$$C_f=\frac{3(1-\frac{R_f-R_m}{R_o-R_m})(1-2L_f/L)}{1-6L_f/L+6(L_f/L)^2}$$

where L_f/L is the relative position of the inflection point for the die and can vary from 0 to 1 [20].

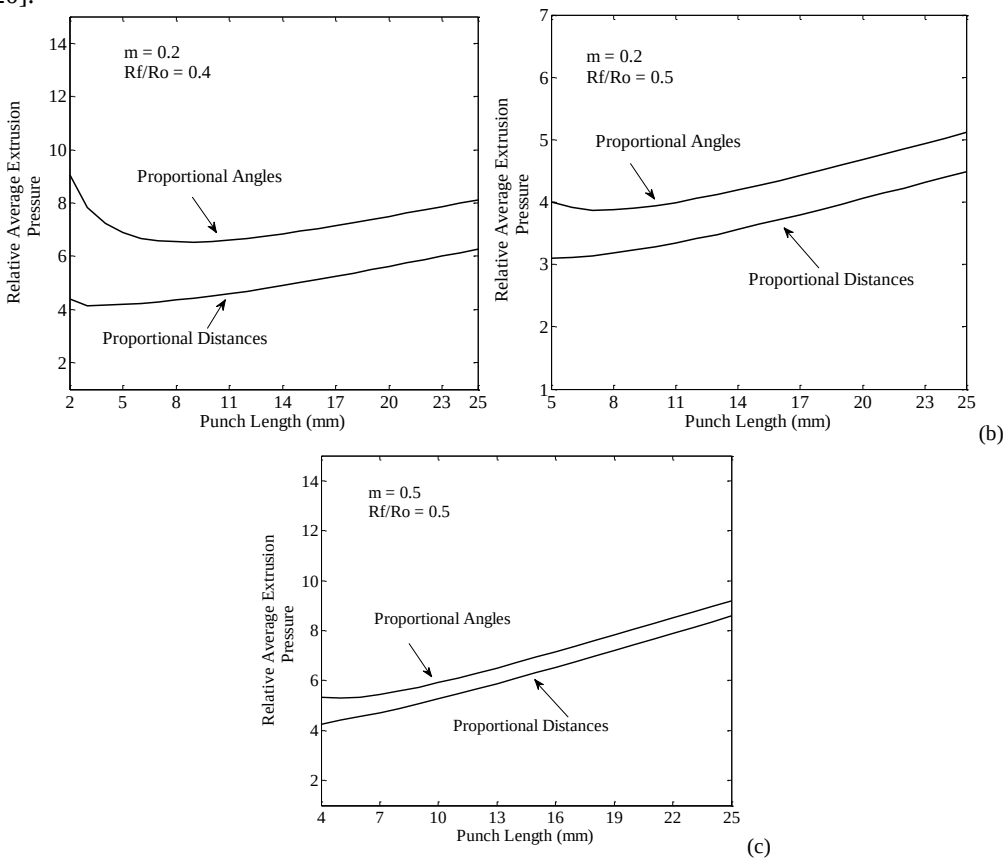

Fig. 2 Relative extrusion pressures for extrusion through a Yang and Han punch shape using the angular and sine velocity fields: (a) for $R_f/R_o=0.4$ and $m=0.2$; (b) for $R_f/R_o=0.5$ and $m=0.2$; (c) for $R_f/R_o=0.5$ and $m=0.5$.

DOI 10.12776/ams.v20i1.214 p-ISSN 1335-1532
e-ISSN 1338-1156

Fig. 2 shows the relative average extrusion pressure calculated from the two velocity fields as a function of the punch length. This figure includes two different tube geometry ($R_f / R_o = 0.4$ for Fig. 2a and $R_f / R_o = 0.5$ for Figs. 2b-2c) and two different friction factors ($m = 0.2$ for Figs. 2a-2b and $m = 0.5$ for Fig. 2c). These figures show that the assuming the proportional distances from mandrel surface provide a lower upper bound solution.

4 Comparison of analytical results with the FEM results and experiment

The backward tube extrusion processes is simulated using the finite element software, ABAQUS. Due to the symmetry of the process, two-dimensional axisymmetric models are used for FEM analyses. In each case, the whole model is meshed with CAX4R elements. **Fig. 3**a illustrates the mesh used to analyze the deformation. Punch, mandrel and container undergo elastic strains only. Thus, it is not necessary to use a fine mesh in these two pieces. However, sufficiently fine meshing is essential in material which undergoes plastic deformation. The container is fixed by applying displacement constraint on its nodes while the punch model is loaded by specifying displacement in the axial direction. Deformed model is shown in Fig. 3b.

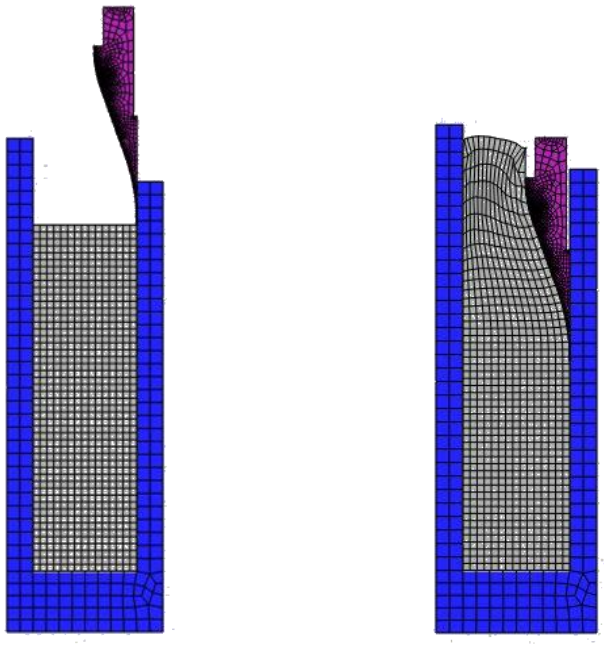

(a) The finite element mesh (b) The deformed mesh

Fig. 3 The finite element mesh and the deformed mesh.

For comparison, the corresponding results are also obtained using experiment. A 50 kN STM universal testing machine is used to perform the experiments, which is illustrated in **Fig. 4**, together with a die-set. A sodium based grease lubricant is applied manually on the contact surfaces of billets and die-sets. The initial tube was lead with length 40 mm, $R_o = 11$ mm, $R_f = 6$, $R_m = 3$ mm and the flow stress given by tensile test as

$$\sigma = 38.97\ \varepsilon^{0.436} \quad \text{(MPa)} \tag{30}$$

DOI 10.12776/ams.v20i1.214 p-ISSN 1335-1532
e-ISSN 1338-1156

Based on Eq. (31) a mean flow stress of 55.5 MPa was estimated for the material used.
The initial tube and the extruded sample corresponding to the conical punch, punch length 8 mm, are shown in **Fig. 5**. Experimental load–displacement curve of the conical punch is shown in **Fig. 6**. By comparing the experimental results of the conical punch with the FEM simulation results, it is found that the shear friction factor m for the experiment is about 0.5 and it is used in upper bound model.

Fig. 4 The 50 kN STM universal testing machine with a die-set mounted.

(a) initial tube (b) conical punch (c) extruded tube

Fig. 5 Initial tube and extruded sample for conical punch.

DOI 10.12776/ams.v20i1.214 p-ISSN 1335-1532
e-ISSN 1338-1156

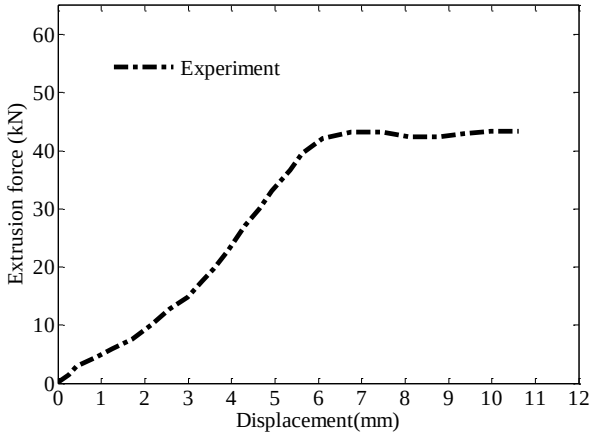

Fig. 6 Experimental force-displacement curve for conical die.

In **Fig. 7**, the analytical, experimental and FEM force-displacement curves for conical punch is compared. The results show good agreement between the analysis and experiment. As shown in this figure, the theoretically predicted extrusion force is higher than the experimental and FEM results, which is due to the nature of the upper bound theory.

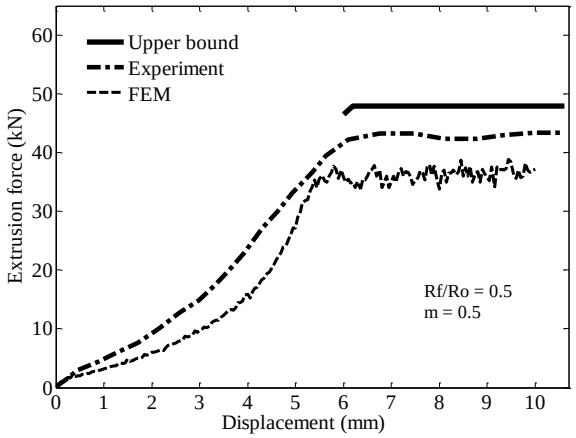

Fig. 7 Comparison between the analytical, experimental and FEM force-displacement curves for conical punch.

Extrusion force variations versus punch length for backward tube extrusion through conical punch and the Yang and Han punch shape obtained from the upper bound model, for $R_f = 6$, mm $R_o = 11$ mm, $R_m = 3$ mm and $m = 0.3$, are compared with each other in Fig. 8. As can be seen from the figure, the trend in the two curves is similar. Also, at any length of the punch, the required extrusion force in the optimum Yang and Han punch shape is less than that in the optimum conical punch.

DOI 10.12776/ams.v20i1.214 p-ISSN 1335-1532
e-ISSN 1338-1156

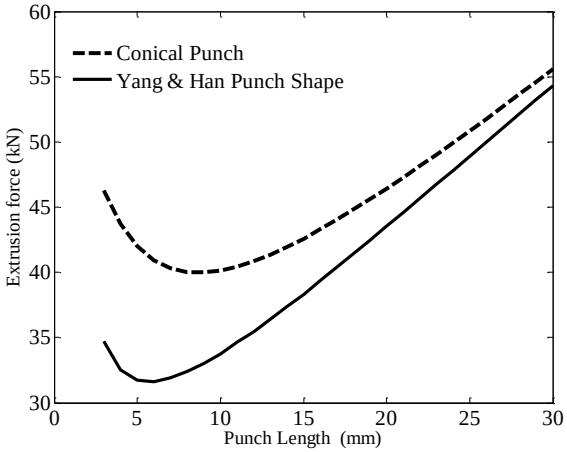

Fig. 8 Comparison between the extrusion force variation versus punch length for conical punch and Yang and Han punch shape obtained from the upper bound ($R_f = 6$ mm, $R_o = 11$ mm, $R_m = 3$ mm and $m = 0.3$)

In **Fig. 9**, the extrusion force displacement curve for optimum Yang and Han punch shape obtained from the upper bound solution and the FEM simulation is compared with each other. The results show good agreement between the analysis and FEM. As shown in this figure, at the early stage of extrusion, unsteady state deformation occurs, and the materials have not yet filled up the cavity of the punch completely. Thus, the extrusion force increases as the extrusion process proceeds. After the materials have filled up the cavity of the punch completely, the extrusion forces are constant. That is because of the frictional surfaces and shear surfaces are no change as the punch is advanced.

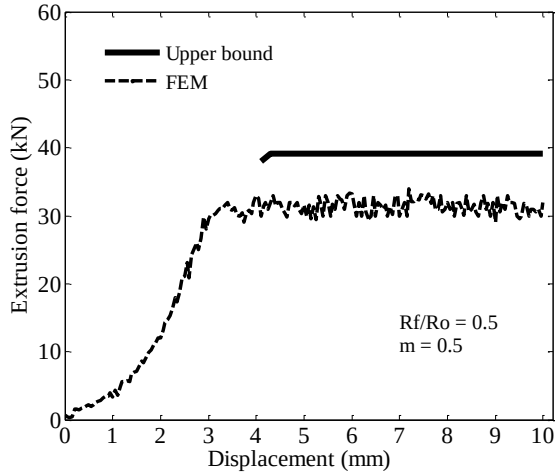

Fig. 9 Comparison of analytical and FEM force-displacement curves for optimum Yang and Han punch shape.

DOI 10.12776/ams.v20i1.214 p-ISSN 1335-1532
e-ISSN 1338-1156

The effect of friction factor upon extrusion force is shown in **Fig. 10**. As shown in these figures, at a punch length that called the optimum length, the extrusion force is minimized. As shown in this figure, the extrusion force increases with increasing the friction factor. Also, with increasing the friction factor, the optimum length of punch is increased.

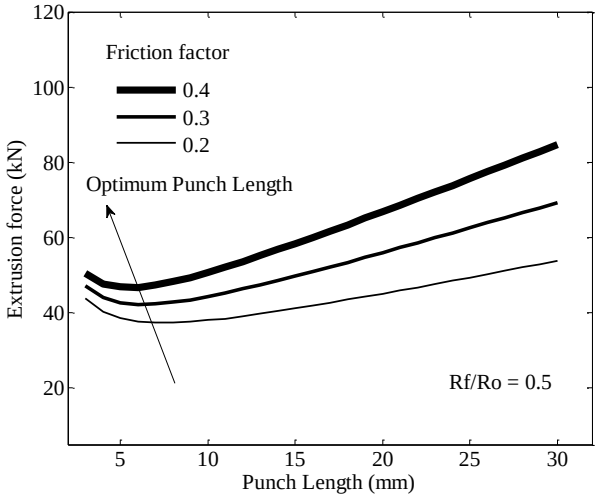

Fig. 10 Effect of friction factor upon the extrusion force for Yang and Han punch shape.

5 Conclusions

In this paper two velocity fields and their power terms for backward tube extrusion process through punches of any shape were presented. Derivations for three main components of the consumed power including deformation, discontinuity and frictional powers were presented. The results of upper bound models for two velocity fields were compared to each other for extrusion through a streamlined die shape. The results demonstrated that assuming proportional distances from the mandrel surface in the deformation zone was better than assuming the proportional angles. Comparison of the measured extrusion force with that estimated by the proposed upper bound solution showed a good agreement. The analytical results were also in good agreement with the FEM data.

The developed upper bound model can be used for finding the optimum punch length which minimizes the extrusion force for a given punch shape and process parameters.

References

[1] B. Avitzur: ASME Journal of Engineering for Industry, Vol. 85, 1963, p. 89–96
[2] B. Avitzur: ASME Journal of Engineering for Industry, Vol. 86, 1964, p. 305–316
[3] B. Avitzur: ASME Journal of Engineering for Industry, Vol. 88, 1966, p. 410–420
[4] C.T. Chen, F.F. Ling: International Journal of Mechanical Sciences, Vol. 10, 1968, p. 863–879
[5] Z. Zimmerman, B. Avitzur: ASME Journal of Engineering for Industry, Vol. 92, 1970, p. 119–129
[6] H.S. Mehta, A.H. Shabaik, S. Kobayashi: ASME Journal of Engineering for Industry, Vol. 92, 1970, p. 403–411

DOI 10.12776/ams.v20i1.214 p-ISSN 1335-1532
e-ISSN 1338-1156

[7] K. T. Chang, J.C. Choi: ASME Journal of Engineering for Industry, Vol. 94, 1972, p. 108–112
[8] C.S. Hartley: International Journal of Mechanical Sciences, Vol. 15, 1973, p. 651–663
[9] D.Y. Yang, C.H. Han, B.C. Lee: International Journal of Mechanical Sciences, Vol. 27, 1985, p. 653–663
[10] D.Y.Yang, C.H. Han: ASME Journal of Engineering for Industry, Vol. 109, 1987, p. 161–168
[11] D. Y. Yang, H.S. Kim, C.M. Lee: CIRP Annuls, Vol. 36, 1987, p. 169-172
[12] D.Y. Yang. H.S. Kim, C.M. Lee, C.H. Han: International Journal of Mechanical Sciences, Vol. 32, 1990, p. 115-127
[13] S.B. Altan: Journal of Material Processing Technology, Vol. 40, 1994, p. 305–313
[14] M. Bakhshi-Jooybari, M. Saboori, S.J. Hosseinipour, M. Shakeri, A. Gorji: Journal of Material Processing Technology, Vol. 177, 2006, p. 596–599, DOI:10.1016/j.jmatprotec.2006.03.194
[15] M. Saboori, M. Bakhshi-Jooybari, M. Noorani-Azad, A. Gorji: Journal of Material Processing Technology, Vol. 177, 2006, p. 612–616, DOI:10.1016/j.jmatprotec.2006.04.031
[16] M. Malpani, S. Kumar: Journal of Material Processing Technology, Vol. 190, 2007, p. 363–374, DOI: 10.1016/j.jmatprotec.2012.01.015
[17] R. Ebrahimi, M. Reihanian, M. Kanaani, M.M. Moshksar: Journal of Material Processing Technology, Vol. 99, 2008, p. 214–220, DOI:10.1016/j.jmatprotec.2007.07.034
[18] W.A. Gordon, C.J. Van Tyne, Y.H. Moon: International Journal of Mechanical Sciences, Vol. 49, 2007, p. 86–95, DOI:10.1016/j.ijmecsci.2006.07.011
[19] W.A. Gordon, C.J. Van Tyne, Y.H. Moon: International Journal of Mechanical Sciences, Vol. 49, 2007, p. 96–103, DOI:10.1016/j.ijmecsci.2006.07.012
[20] W.A. Gordon, C.J. Van Tyne, Y.H. Moon: International Journal of Mechanical Sciences, Vol. 49, 2007, p. 104–115, DOI:10.1016/j.ijmecsci.2006.07.013

Nomenclature

J^*	externally supplied power of deformation
m	constant friction factor
k	material yield strength in shear
L	punch length
L_f	bearing length
r, θ, ϕ	spherical coordinate system
r_f	radial position of the velocity discontinuity surface S_2
r_o	radial position of the velocity discontinuity surface S_1
S	area of frictional or velocity discontinuity surface
V_r, V_θ, V_ϕ	radial, angular and third components of velocity
V	volume of integration
V_f	velocity of final tube
V_o	velocity of punch
$\dot{W}_{f3}, \dot{W}_{f4}, \dot{W}_{f5}, \dot{W}_{f6}$	frictional power losses along the frictional surfaces S_3, S_4, S_5 and S_6, respectively
$\dot{W}_i$	internal power of deformation

DOI 10.12776/ams.v20i1.214 p-ISSN 1335-1532
e-ISSN 1338-1156

$\dot{W}_{S1}, \dot{W}_{S2}$	shear power losses along the velocity discontinuity surfaces S_1 and S_2 , respectively
α	angle of the line connecting the initial point of the punch to the final point of the punch
ΔV	velocity difference
$\dot{\varepsilon}_{rr}$, $\dot{\varepsilon}_{\theta\theta}$, $\dot{\varepsilon}_{\phi\phi}$	normal strain rate components
$\dot{\varepsilon}_{r\theta}$, $\dot{\varepsilon}_{r\phi}$, $\dot{\varepsilon}_{\theta\phi}$	shear strain rate components
η	local angle of the punch surface with respect to the local radial velocity component
σ	flow stress of the workpiece material
σ_0	mean flow stress of the workpiece material
τ	frictional shear stress
ψ	angular position of the punch surface as a function of radial position

DOI 10.12776/ams.v20i1.214 p-ISSN 1335-1532
e-ISSN 1338-1156